

See discussions, stats, and author profiles for this publication at: <https://www.researchgate.net/publication/320697836>

Reduced graphene oxide modified NiFe-calcinated layered double hydroxides for enhanced photocatalytic removal of methylene blue

Article in *Applied Surface Science* · October 2017

DOI: 10.1016/j.apsusc.2017.10.181

CITATIONS

3

READS

69

7 authors, including:

[Guoqing Zhao](#)

Central South University

4 PUBLICATIONS 4 CITATIONS

SEE PROFILE

[Wenjiahao hu](#)

University of Alberta

7 PUBLICATIONS 14 CITATIONS

SEE PROFILE

Full Length Article

Reduced graphene oxide modified NiFe-calcinated layered double hydroxides for enhanced photocatalytic removal of methylene blue

Guoqing Zhao^a, Caifeng Li^a, Xia Wu^a, Jingang Yu^a, Xinyu Jiang^a, Wenjihao Hu^{a,b,*}, Feipeng Jiao^{a,**}^a School of Chemistry and Chemical Engineering, Central South University, Changsha, 410083, People's Republic of China^b Department of Chemical and Material Engineering, University of Alberta, Edmonton, T5K1B9, Canada

ARTICLE INFO

Article history:

Received 28 June 2017

Received in revised form 9 October 2017

Accepted 26 October 2017

Available online 28 October 2017

Keywords:

Photocatalytic degradation
RGO/NiFe-CLDH composites
MB

ABSTRACT

Calcined layered double hydroxides (CLDH) are one of the remarkable photocatalysts passionately studied for photodecolorization of organic dyes. NiFe-CLDH was successfully modified by reduced graphene oxide (RGO) through a facile in situ crystallization technique. The obtained RGO/NiFe-CLDH composites were fully characterized by powder X-ray diffraction (XRD), Scanning electron microscopy (SEM), high-resolution transmission electron microscopy (HRTEM), Fourier transform infrared (FT-IR), and UV–vis diffuse reflectance spectroscopy (DRS). The results analysis indicated that RGO sheets could work as base course to prompt the growth of LDH crystallites and NiFe-LDH lamellar crystal promiscuously distributed on the sheets with a strong interplay between each other. The photocatalytic performance of RGO/NiFe-CLDH composites toward decolorization of methylene blue tightly depended on the mass fraction of RGO and calcination temperature. At the RGO weight loading of 1%, calcination temperature of 500 °C, the photocatalytic degradation efficiency of RGO/NiFe-CLDH composites reached 93.0% within 5.0 h. The enhanced activity of RGO/NiFe-CLDH composites may be due to the concerted catalysis effect between two constituents of as-prepared composites.

© 2017 Published by Elsevier B.V.

1. Introduction

Up to now, water pollution is a significant component of environmental focus and becomes a main problem to be settled for a better of human health. However, the polluted wastewater is extensively generated as effluents from various industries including paper, petrochemical, and plastics [1]. However, most of the dyes, as a typical organic polluted wastewater, are hard to remove by conventional technologies [2]. As we all know, various technologies have been developed to remove the polluted wastewater, such as adsorption, membranes separation and filtration etc. Among them, photocatalytic degradation is considered as the most high-efficiency and promising methods for the removal of dyes. Clearly, the main research challenge of degradation methods is the selection of suitable photocatalysts materials.

In recent decades, semiconductor photocatalysts, as promising photocatalysts, have been broadly attention on the field of environmental pollution treatment and solar energy conversion since Japanese scholar developed the photocatalysis [3]. Especially in pollutants photocatalytic degradation, photocatalysis treatment methods have some advantages, such as low toxicity, high mineralization efficiency, fast photocatalysis degradation efficiency, etc. Therefore, recent years have gone through widely attention on the design and fabrication of semiconductor-based photocatalytic materials. Hence, various semiconductor-based catalysts containing TiO₂, ZnO, AgX (Cl, Br, I), were developed for the photocatalytic degradation of organic wastewater [4,5]. Among these widely studied photocatalysts, layered double hydroxides are one of the most fruitful materials for photocatalytic degradation of organic wastewater into harmless substance [6,7].

Layered double hydroxides (LDH), also known as hydrotalcite-like compounds, are a kind of inorganic anionic clays consisting of host-guest layered solids and exchangeable interlayer anions, which can be normative expressed by the general formula $[M^{2+}_{1-x}M^{3+}_x(OH)_2]^{x+}(A^{n-})_{x/n} \cdot mH_2O$, where M^{2+} and M^{3+} represent di- and trivalent metal anions, respectively, and A^{n-} denotes the interlayer organic and inorganic anions, x is calculated by

* Corresponding author at: Department of Chemical and Material Engineering, University of Alberta, Edmonton, T5K1B9, Canada.

** Corresponding author at: School of Chemistry and Chemical Engineering, Central South University, Changsha, 410083, People's Republic of China.

E-mail addresses: huwenjihao@163.com (W. Hu), jiaofp@163.com (F. Jiao).

$M^{2+}/(M^{2+} + M^{3+})$, m is the number of crystal water on the inter-layer [8,9]. Owing to the flexible chemical composition and uniform structure architecture, both LDH and their calcined layered double hydroxides (CLDH) have been extensively application on photocatalytic CO_2 -reduction and photodegradation of organic pollutants [10,11]. Liu et al. demonstrated that a series of novel TiO_2 - $BiOCl$ - $ZnCr$ -Ex composites were a re-usability photocatalyst for degradation of organic pollutants in wastewater treatment [12]. Meng et al. reported salen-metal complexes (metal = Co or Ni) intercalated $ZnCr$ -LDHs displayed excellence photocatalytic activity for the decolorization of Rhodamine B under visible light illumination, much better than that of commercial catalysts [13]. Meanwhile, most reported calcinated layered double hydroxides (CLDH) and its hybrid materials are developed in recent years [14–16]. However, only several very recent reports validated that $NiFe$ -CLDH itself or modified $NiFe$ -CLDH showed photocatalytic activity toward dyes wastewater [17,18]. Nevertheless, in order to expand CLDH based photocatalysts driven by visible light, it is necessary to investigate the appropriate semiconductor materials.

Till now, RGO, as semiconductor photocatalysts, has gained wide attention due to their high adsorption, large specific area and good charge transfer performance as well as its remarkable chemical stability and displays excellent photocatalytic activities toward mounts of dyes pollutants [19]. So, RGO was widely used to be coupled composites to improve photocatalytic performance of the objective products [20]. Hence, in this study, $RGO/NiFe$ -CLDH composites were successfully prepared via a facile in situ crystallization technique. The as-prepared samples were characterized by XRD, SEM, UV-vis DRS, FT-IR and their photocatalytic properties were investigated by MB stimulation wastewater. More important, the possible photodegradation mechanism was also proposed in the paper.

2. Experimental

2.1. Materials

The raw chemical materials $Ni(NO_3)_2 \cdot 6H_2O$, $Fe(NO_3)_3 \cdot 9H_2O$, $NaOH$, H_2SO_4 , anhydrous Na_2CO_3 , HNO_3 , H_2O_2 , potassium permanganate ($KMnO_4$), ascorbic acid, *L*-tryptophan, absolute ethanol, methylene blue (MB) and graphite powders were of analytical reagent grade and used as received and without further purification.

2.2. Synthesis of GO

GO was synthesized by the modified Hummers' methods and the typical synthesis process was the same as Bai's previous reported [19].

2.3. Synthesis of RGO

In a typical synthesis of RGO nanosheets, 0.040 g of above prepared GO, 0.80 g of *L*-tryptophan, 2.0 g of ascorbic acid, 0.16 g of $NaOH$ and 400 mL of distilled water were added into a round bottom flask, followed sonication for 10 min to formed brown solution. After that the round bottom flask was maintained at $80^\circ C$ for 48 h under the oil-bath. Finally, the resulting dark solids were recovered by filtration, washed with DI water, and fully dried at $60^\circ C$.

2.4. Synthesis of $RGO/NiFe$ -CLDH composites

$RGO/NiFe$ -CLDH composites with different RGO loadings were prepared by in situ coprecipitation of $NiFe$ -CLDH (Ni/Al molar ratio of 3) onto RGO according to a simple procedure. Typically, RGO

dispersions were prepared by dissolving a certain amount of RGO into 80 mL distilled water under the aid of ultrasonication. Then 1.45 g of $Ni(NO_3)_2 \cdot 6H_2O$ (0.005 mol) and 0.675 g of $Fe(NO_3)_3 \cdot 9H_2O$ (0.00167 mol) were dispersed in the above dispersions by ultrasonication another 30 min. After that, the dispersions were located on the magnetic stirrers. During the experiment, the pH of the solution was kept at 8–9 by simultaneous addition of 1.0 mol/L $NaOH$. Afterwards, the resulting products were hydrothermal treated at the temperature of 333 K for 48 h and then washed with distilled water and ethanol several times. Then the products were dried overnight at 333 K in vacuum. The as-prepared samples were defined as X - $RGO/NiFe$ -LDH, where X represents the weight percentage of RGO in composites and in this paper, X values are 0.5%, 1%, 2% and 3%, respectively. Then, the $RGO/NiFe$ -LDH samples were calcined in vacuum at $400^\circ C$, $500^\circ C$, and $600^\circ C$ for 4 h in a tube furnace to obtain the $RGO/NiFe$ -CLDH-400, $RGO/NiFe$ -CLDH-500 and $RGO/NiFe$ -CLDH-600, respectively.

2.5. Characterization

The phase and crystal structure of the prepared composites were investigated by X-ray diffractometer (XRD, Bruker D8) using $Cu K\alpha$ radiation ($\lambda = 1.5406 \text{ \AA}$, 40 KV, 40 mA). The morphology and microscopy of the products were checked by scanning electron microscopy (SEM, TESCAN MIRA3 LMU) and high-resolution transmission electron microscopy (HRTEM, JEOL JEM-2100F, voltage of 200 kV). Samples for HRTEM measurements were prepared by sonicating the products in ethanol for 30 min and evaporating a drop of the resulting suspension onto a copper grid. The elementary compositions were conducted by Energy dispersive X-ray (EDX) analysis attached to the TESCAN MIRA3 LMU devices. The UV-vis diffused reflectance spectra (DRS) of the sample powers were investigated by a UV-vis spectrophotometer (Shimadzu 2401 spectrophotometer). Fourier transform infrared (FT-IR) spectra were recorded using an AVATAR 360 spectrometer (Nicolet instrument Corporation, America) in the 4000 – 400 cm^{-1} .

2.6. Photocatalytic activity test

The photocatalytic activity of the prepared samples was investigated for methylene blue (MB) photocatalytic degradation. The photocatalytic experiments were examined by adding 50 mg $RGO/NiFe$ -CLDH composites powder into a glass tube with a circulating water jacket containing 50 mL of the simulation wastewater. Before turning on the visible light, the suspension was located under the magnetic stirrer in dark for 1 h to reach an adsorption-desorption equilibrium. After that, a 500 W xenon lamp ($\lambda \geq 420 \text{ nm}$) was opened as visible light source. During the visible light irradiation, 3 mL of the suspension solution was extracted at every 1 h intervals and then filtered to remove the catalysts from the solution. The MB concentration in the filtrated solution was determined using UV-vis spectrophotometer (UV-9600) at 554 nm.

3. Results and discussion

3.1. Characterization of $RGO/NiFe$ -CLDH composites

3.1.1. XRD

Fig. 1 shows the XRD patterns of $NiFe$ -CLDH-500, bulk RGO, $NiFe$ -LDH, and $RGO/NiFe$ -LDH with different RGO loadings and calcination temperature. RGO appeared one reflections at around 25.6° indexed as the (002) crystal planes of RGO. For the patterns of the products, the peaks at $2\theta = 11.38^\circ$, 22.99° , 33.50° , 38.38° and 61.26° are attributed to the (003), (006), (012), (015) and (110) planes of $NiFe$ -LDH [18]. The existence of the (003) and (006) can be regarded as the incorporation of CO_3^{2-} ions and H_2O molecules

Fig. 1. The XRD patterns of (Aa) NiFe-CLDH-500 (Ab) RGO (Ac)NiFe-LDH (Ad)RGO-LDH (Ae)RGO/NiFe-CLDH-500 (Ba) RGO/NiFe-CLDH-400 (Bb) RGO/NiFe-CLDH-500 (Bc) RGO/NiFe-CLDH-600 composites.

within the LDH lattice. Besides, the d -spacing corresponding to the (003) peak was found to be 0.769 nm. For all the composites, the characteristic (002) diffraction of RGO was hardly appeared. This was due to the formed RGO exfoliated in the LDH crystals. As shown in Fig. 1(B), the reflections were found at $2\theta = 37.25^\circ, 43.28^\circ, 62.87^\circ, 75.41^\circ$ and 79.22° corresponding to (111), (200), (220), (311) and (222) of the CLDH. By comparison, the characteristic diffraction of NiO was discovered (JCPDF.64-6098), demonstrating the structure of the LDH slashstone floor collapsed at the calcination temperature of 500°C . Furthermore, with increasing the calcination temperature, the NiO and NiFe_2O_4 (JCPDF.5-2387) components were obtained, which could be considered as the nickel-iron spinel formed at higher calcination temperature.

3.1.2. SEM, EDX and TEM analysis

The SEM images of the RGO/NiFe-CLDHs composites, pure RGO and RGO/NiFe-LDH are all displayed in Fig. 2. From Fig. 2A, it can be seen that RGO has obvious flake-like wrinkled structure and displays disorder status. This is a typical morphology of RGO structure [21]. It could be found from Fig. 2B that NiFe-LDH sheets were well-dispersed on the supporting flake-like wrinkled RGO sheets, which can be ascribed to the dedication of hydrothermal treatment [22]. The lamellar RGO/NiFe-LDH structures having a lateral diameter of about 200–300 nm could be seen in the SEM images. From Fig. 2C, we can find that the layer structure of the samples was disappeared, which due to the RGO/NiFe-LDH may layer structure collapsed under the higher calcination temperature. Furthermore, the small mixed metal oxide particles were well-uniform-dispersed on the supporting RGO sheets, which greatly reduced the reuniting of the metal oxides. Meanwhile, the EDX of RGO/NiFe-CLDH composites is shown in Fig. 2D, where the elements of C, O, Ni, and Fe are observable, further indicating that RGO/NiFe-CLDH was synthesized successfully. The Fig. 2E and F were also clearly noted that uniform nanoplates with uniform sizes were even dispersed on the surface of flexible and transparent grapheme sheets, suggestive of the high structural matching degree and good contacted with them. Closely inspection of a representative HRTEM image depicted the interplanar distance of about nm for an individual NiFe-LDH nanoplatelet in the RGO/NiFe-LDH composites. Under the present synthetic conditions, layer double hydroxides were first adsorbed on the surface of RGO via hydrothermal method, and then NiFe-LDH nuclei were uniformly formed on the surface of RGO.

3.1.3. FT-IR

The FT-IR spectra (Fig. 3) of RGO/NiFe-CLDH composites was analyzed and compared with pure GO, RGO, and RGO/NiFe-LDH including hydroxyl species, carboxylic species, and epoxy species etc. Typically, from Fig. 3a, the broad absorption peaks about 3427 cm^{-1} is due to the $-\text{OH}$ stretching vibration [23]. The strong peak at nearly 1703 cm^{-1} , 1623 cm^{-1} , 1224 cm^{-1} , 1056 cm^{-1} , corresponded to the vibrational absorption of $\text{C}=\text{O}$ stretching vibration, $\text{C}=\text{C}$ stretching vibration, $\text{C}-\text{OH}$ stretching vibration and $\text{C}-\text{O}$ stretching vibration, respectively. As for Fig. 3c, the absorption peaks of 3427 cm^{-1} , 1703 cm^{-1} , 1224 cm^{-1} , and 1056 cm^{-1} are bated showing that the oxygen functional groups on the surface of GO were removed. Compared with NiFe-LDH and NiFe-CLDH [22], all characteristic peaks of LDH can be found in the spectrum of RGO/NiFe-CLDH and the decreased characteristic peak intensities of RGO/NiFe-CLDH are due to the change of RGO. Beside, the FT-IR spectrum of Fig. 3d shows characteristic peak 1357 cm^{-1} , compared with RGO-LDH, indicating that there has CO_3^{2-} in the interlayer of RGO/NiFe-CLDH. The characteristic peak at 1623 cm^{-1} is appeared, which indicated that RGO is located on the LDH successfully. Meanwhile, the characteristic peaks at 412 cm^{-1} is attributed to Ni–O vibration peaks. Hence, it is corresponding to the characteristic of XRD and SEM.

3.1.4. UV-vis DRS

Fig. 4A a–d shows UV-vis diffuse reflectance spectra of the RGO/NiFe-LDH, NiFe-CLDH-500, GO/NiFe-CLDH-500 and RGO/NiFe-CLDH-500. As we can see, the spectrum of NiFe-CLDH-500 shows stronger UV light ($\lambda < 400\text{ nm}$) adsorption ability. The adsorption edge of pure NiFe-CLDH-500 composites is located at around 348 nm, which agrees with the previous reported [18]. Compared with the NiFe-CLDH-500 with broad absorbance over the whole visible region, the visible absorption intensity of GO/NiFe-CLDH-500 and RGO/NiFe-CLDH-500 are noticeably improved, which is showed that the absorption peaks of the products are red-shifted in the wavelength range from 360 nm to 510 nm, indicating that the GO and RGO introduction enhances the visible light adsorption. The optical band gap energies (E_g) of a single semiconductor can be estimated by the formula $A(h\nu) - E_g = (ah\nu)^{1/n}$. The n value represents dependent on the type of a semiconductor ($n = 1/2$ for direct semiconductor and $n = 2$ for indirect semiconductor). Hence, as found in Fig. 4B, the band gaps of RGO/NiFe-CLDH-500 compos-

Fig. 2. SEM image of (A) RGO (B) RGO/NiFe-LDH (C) RGO/NiFe-CLDH-500 composites and EDX spectra of (D) RGO/NiFe-CLDH-500 composites. TEM (E) images of RGO/NiFe-LDH and HRTEM (F) image of an individual NiFe-LDH nanoparticle on the RGO surface.

Fig. 3. FT-IR spectrum of (a) RGO/NiFe-LDH (b) GO (c) RGO (d) RGO/NiFe-CLDH-500 composites.

Fig. 4. (A) UV-vis DRS of (a) RGO/NiFe-LDH (b) NiFe-CLDH-500 (c) GO/NiFe-CLDH-500 and (d) RGO/NiFe-CLDH-500 composites; (B) Calculated band gap energies of RGO/NiFe-CLDH-500 composites.

ites are estimated to be 2.82 eV. The obtained composites exhibits the good adsorption intensity in the visible light region, which will enable improve the photocatalytic activity of the obtained composites.

Fig. 5. Comparative studies of the photocatalytic activity of the various catalysts under visible light.

3.2. Photocatalytic activity of the products

3.2.1. Effect of various photocatalysts

The photocatalytic activity of different photocatalysts was investigated by the removal of MB under visible light irradiation. Fig. 5 shows the photocatalytic activity of NiFe-LDH, NiFe-CLDH-500, GO/NiFe-LDH, RGO/NiFe-LDH, GO/NiFe-CLDH-500 and RGO/NiFe-CLDH-500 composites. The blank test demonstrated the concentration of MB keeps no significant change without any photocatalysts under the same conditions, suggesting that MB is difficult to be self-degraded. The adsorption capacity of MB on the samples was studied in the darkroom conditions and proved that the suspensions reach the adsorption-desorption equilibrium. The results show the decreased concentration of MB is nearly the same for all products, indicating that the experimental photocatalysts have similar adsorption capacity of MB. Then, putting the catalysts and MB stimulation wastewater under visible light irradiation for 4 h, 38.8%, 47.7%, 55.2%, 57.1%, 76.9% and 93.0% of MB removal are achieved over NiFe-LDH, NiFe-CLDH-500, GO/NiFe-LDH, RGO/NiFe-LDH, GO/NiFe-CLDH-500, and RGO/NiFe-CLDH-500 composites, respectively, indicating the composites have good photocatalytic activity. However, only 38.8% of the MB was removed by pure NiFe-LDH under the same reaction conditions, which shows that the photocatalytic efficiency of pure NiFe-LDH composites is relatively poor. The good activity of RGO/NiFe-CLDH-500 composites may be ascribed to the well-uniform-dispersed small mixed metal oxide particles and the bigger surface supported RGO sheets, which was constant with the above SEM images. Besides, the special structure was best for the generation of electrons and holes.

3.2.2. Effect of catalysts with different mass ratios of RGO

The effect of catalysts with different mass ratios on the photocatalytic activity of RGO/NiFe-CLDH composites was shown in Fig. 6. It is obvious observed that the degradation percentage of MB is 85.7%, 93.0%, 88.7%, and 82.6% within 5 h at different RGO mass ratios 0.5%, 1.0%, 2.0%, and 3.0%, respectively. From Fig. 6, it clearly finds that the RGO/NiFe-CLDH composites catalysts show the remarkable color removal efficiency at the RGO mass ratios of 1.0% than the others. However, the RGO can transfer electrons in the process of photocatalysts. The lower degradation efficiency of RGO/NiFe-CLDH at the RGO mass ratio of 0.5% may be attributed to the smaller loading of RGO in composites which reduced the charge transfer rates of photocatalysts. On the other hand, the RGO mass ratios of 2.0% and 3.0% loading composites display bad degradation

Fig. 6. The photocatalytic activity of catalysts with different mass ratios of RGO under visible light irradiation.

efficiency, which is due to the electrons transfer and energy transfer or mounts of photoinduced electrons and holes are recombined. Besides, the dark materials can decrease the visible light adsorption and restrain the electrons and holes generated on the surface of NiO.

3.2.3. Effect of various calcination temperature

The effect of various calcination temperatures on the photocatalytic activity of samples is displayed in Fig. 7. It is clearly observed that the degradation efficiency of MB is 88.8%, 93.0%, and 43.8% within 4 h at different calcination temperature 400 °C, 500 °C, and 600 °C, respectively. Obviously, RGO/NiFe-CLDH-500 displayed the highest photocatalytic degradation efficiency among all products. The experimental results proved that the calcination temperature had a dominant effect on the photocatalytic performance. On the lower calcination temperature, the poor crystal structure formed leads to the lower photocatalytic activity. However, at higher calcination temperature, mounts of NiFe₂O₄ spinel are formed resulting in the photocatalytic activity decreased. Hence, the RGO/NiFe-CLDH-500 composites are the aimed samples and it was needed to investigate the products in follow-on experiments.

Fig. 7. The photocatalytic activity of various calcination temperatures under visible light irradiation.

Fig. 8. Effects of initial concentration of MB on the photocatalytic activities in the presence of RGO/NiFe-CLDH-500 composites.

Table 1

The pseudo-first-order rate constants of photocatalytic degradation.

C ₀ (mg/L)	Kinetic equations	K _a (min ⁻¹)	R ²	t _{1/2} (min)
5	Y = -2.041X	2.041	0.99519	0.340
10	Y = -0.642X	0.642	0.99926	1.080
15	Y = -0.236X	0.236	0.99991	2.939

3.2.4. Effect of various MB concentration

The photocatalytic activity of RGO/NiFe-CLDH-500 composites was investigated by the degradation efficiency of MB under visible light irradiation at room temperature. Moreover, the effect of MB concentration on the photocatalytic activity of samples was shown in Fig. 8. In our work, the effect of initial MB concentration on degradation efficiency was investigated by varying the initial MB concentration of 5 mg/L, 10 mg/L, and 15 mg/L (V_{MB} = 50 mL, m_{samples} = 50 mg, pH = 7.0) at room temperature, respectively. As found in Fig. 8, the photodegradation rate of MB decreased from 98.2%, 93.0%, and 61.1% to with the increase of the original MB concentrations from 5 mg/L, 10 mg/L, and 15 mg/L.

In order to quantitatively characterized the kinetic behaviors of photodegradation of MB dye in aqueous solution, the experimental data corresponding to the Langmuir–Hinshelwood model, which can be studied by the following equation [24].

$$\ln \frac{C_0}{C} = k_a t \quad (1)$$

$$t_{1/2} = \frac{\ln 2}{k_a} \quad (2)$$

Where, C₀ represents the original concentration of MB (mg/L), C is MB concentration (mg/L) at instantaneous time t and k_a stands for the apparent pseudo-first-order rated constant (h⁻¹). The results were presented in Figs. 9–10 and Table 1. From Fig. 9 and Table 1, the higher values of the linear regression coefficients (R²) indicate that the photocatalytic reaction is well matched with the pseudo-first-order reaction kinetic, despite the difference in the initial MB concentration. For Fig. 10, it was obvious that the decrease of the rate constant k_a with the increase in MB concentration is observed. Thinking about above results, the possible reason may be attributed to the mounts of MB molecules covered on the surface of the photocatalysts at higher initial MB concentration, which blocks the adsorption of light on the surface of the catalysts. To some extent, the results confirm that the MB concentration 10 mg/L is the optimum degradation concentration for the as-prepared photocatalysts.

Fig. 9. Effects of initial MB concentration on the degradation of MB by RGO/NiFe-CLDH-500 composites at pH 7.0 under visible light irradiation.

Fig. 10. Apparent rate constants for the degradation of MB by RGO/NiFe-CLDH-500 composites at pH 7.0 under visible light irradiation.

3.3. Photocatalytic stability of samples

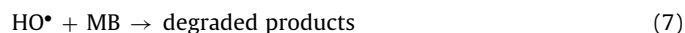
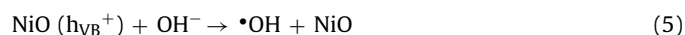
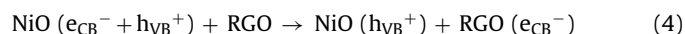
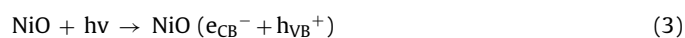
Apart from photocatalytic activity, the stability and reusability of photocatalysts are also key points to their practical application [25]. The stability of the as-obtained RGO/NiFe-CLDH-500 composites photocatalysts was also evaluated according to the same process as mentioned above. After every 5.0 h of photodegradation process, the catalysts were recycled by centrifugation, washed with absolute ethanol and distilled water, and reused in next cycle. As found in Fig. 11, the photocatalytic activity of RGO/NiFe-CLDH-500 composites still conserve 80% of its initial activity after being recycled for four times, which indicates that the catalysts possess remarkable reusability for potential practical applications in environmental purification.

3.4. Photocatalytic mechanism of photocatalysts

Based on these results, the detailed mechanisms of RGO/NiFe-CLDH-500 composites for the MB degradation are proposed in Fig. 12. In this photocatalytic procedure, a series of photo-induced reactive species containing h^+ , $\bullet OH$, and $\bullet O_2^-$, are suspected to be involved in the photocatalytic degradation reaction. In general, the RGO and NiO components played the key catalytic active substance

Fig. 11. Photocatalytic cycles of RGO/NiFe-CLDH-500 composites at pH 7.0 under visible light irradiation.

in RGO/NiFe-CLDH-500 composites. The single RGO and NiO will be excited to produce photoinduced electron-hole pairs under the visible light irradiation. As the visible light driven system, the electron and hole pairs were formed in the as-prepared composites photocatalysts. Besides, it can be well proved that the NiO regarded as the electrons donors and RGO played an electron acceptor. In this composites structure, the electrons in the conduction band (CB) of the NiO was rapidly transferred to the conduction band (CB) of RGO since the CB level of RGO is lower than that of NiO. Meanwhile, the electrons and holes were effectively separated. Therefore, the electrons were transferred from the active point to the surface of RGO/NiFe-CLDH-500 composite, where they react with combining or dissolved oxygen to produce highly reactive superoxide radical anion, at the same time, the holes oxidized H_2O or $-OH$ to $\bullet OH$ radicals [26]. At last, mounts of active species reacted with the MB molecules to form harmless molecules. All in all the photocatalytic degradation process may be described the following reactions of (3)–(8).



4. Conclusion

In this paper, typical RGO/NiFe-CLDH composites are prepared by simple methods. Series of characterization manifest that RGO/NiFe-CLDH composites are higher crystalline powders and higher utilization of visible light and more efficient separation of electron-hole pair. Then, the photocatalysts were used to study the essence of elimination of MB dye pollutants from water solution. In comparison with the pure NiFe-LDH, NiFe-CLDH, GO/NiFe-LDH, and GO/NiFe-CLDH, the RGO/NiFe-CLDH composites improve the photocatalytic activity for the photodegradation of MB dye under visible light irradiation. Results show that the composites have a good photocatalytic activity (93.0%) at the optimum of synthesis composites. Furthermore, the degradation ratio of MB is still having

Fig. 12. Mechanism scheme for MB degradation promoted by RGO/NiFe-CLDH-500 photocatalyst under visible light irradiation.

more than 80% after four cycle runs. Meanwhile, the possible mechanism and synthesis conditions reported could be easily imitated to synthesize other materials for different applications.

Acknowledgements

The authors would like to thank National Science Foundation of China (Grant No. 21476269, 21776319), and the Fundamental Research Funds for the Central Universities of Central South University (Grant No. 2017zzts777) for the financial supports of this work.

References

- [1] J.S. Zhang, T.J. Yao, C.C. Guan, N.X. Zhang, H. Zhang, X. Zhang, J. Wu, One-pot preparation of ternary reduced graphene oxide nanosheets/Fe₂O₃/polypyrrole hydrogels as efficient Fenton catalysts, *J. Colloid Interface Sci.* 505 (2017) 130–138.
- [2] C.L. Yu, Z. Wu, R.Y. Liu, D.D. Dionysious, K. Yang, C.Y. Wang, H. Liu, Novel fluorinated Bi₂MoO₆ nanocrystals for efficient photocatalytic removal of water organic pollutants under different light source illumination, *Appl. Catal. B: Environ.* 209 (2017) 1–11.
- [3] M.A. Henderson, I. Lyubintsky, Molecular-level insights into photocatalysis from scanning probe microscopy studies on TiO₂ (110), *Chem. Rev.* 113 (2013) 4428–4455.
- [4] J. Fei, J. Li, Controlled preparation of porous TiO₂-Ag nanostructures through supramolecular assembly for plasmon-enhanced photocatalysis, *Adv. Mater.* 27 (2015) 314–319.
- [5] C. Dong, K.L. Wu, X.W. Wei, J. Wang, L. Liu, B.B. Jiang, Nitrogen-doped graphene modified AgX@Ag (X = Br, Cl) composites with improved visible light photocatalytic activity and stability, *Appl. Catal. A: Gen.* 488 (2014) 11–18.
- [6] Z.H. Li, M.F. Shao, L. Zhou, R.K. Zhang, C. Zhang, J.B. Han, M. Wei, D.G. Evans, X. Duan, A flexible all-solid-state micro-supercapacitor based on hierarchical CuO@layered double hydroxide core-shell nanoarrays, *Nano Energy* 20 (2016) 294–304.
- [7] S.J. Xia, F.X. Liu, Z.M. Ni, J.L. Xue, P.P. Qian, Layered double hydroxides as efficient photocatalysts for visible-light degradation of Rhodamine B, *J. Colloid Interface Sci.* 405 (2013) 195–200.
- [8] R.Z. Liang, R. Tian, W.Y. Shi, Z.H. Liu, D.P. Yan, M. Wei, D.G. Evans, X. Duan, A temperature sensor based on CdTe quantum dots-layered double hydroxide ultrathin films via layer-by-layer assembly, *Chem. Commun.* 49 (2013) 969–971.
- [9] F.P. Jiao, J.G. Yu, H.L. Song, X.Y. Jiang, H. Yang, S.Y. Shi, X.Q. Chen, W.J. Yang, Excellent adsorption of acid flavine 2G by MgAl-mixed metal oxides with magnetic iron oxide, *Appl. Clay Sci.* 101 (2014) 30–37.
- [10] M. Zhang, B. Gao, Y. Yao, M.D. Inyang, Phosphate removal ability of biochar/MgAl-LDH ultra-fine composites prepared by liquid-phase deposition, *Chemosphere* 92 (2013) 1042–1047.
- [11] K. Teramura, S. Iguchi, Y. Mizuno, T. Shishido, T. Tanaka, Photocatalytic conversion of CO₂ in water over layered double hydroxides, *Angew. Chem. Int. Ed.* 51 (2012) 8008–8011.
- [12] Q. Liu, J.F. Ma, K. Wang, T. Feng, M.G. Peng, Z.S. Yao, C.H. Fan, S. Komarneni, BiOI and TiO₂ deposited on exfoliated ZnCr-LDH to enhanced visible-light photocatalytic decolorization of Rhodamine B, *Ceram. Int.* 43 (2017) 5751–5758.
- [13] Y. Meng, W. Luo, S.J. Xia, Z.M. Ni, Preparation of salen-metal complexes (metal = Co or Ni) intercalated ZnCr-LDHs and their photocatalytic degradation of Rhodamine B, *Catalysts* 7 (2017) 143–157.
- [14] R.R. Shan, L.G. Yan, K. Yang, S.J. Yu, Y.F. Hao, H.Q. Yu, B. Du, Magnetic Fe₃O₄/MgAl-LDH composite for effective removal of three red dyes from aqueous solution, *Chem. Eng. J.* 252 (2014) 38–46.
- [15] J.C. Sun, H. Fan, B. Nan, S.Y. Ai, Fe₃O₄@LDH/Ag/Ag₃PO₄ submicrosphere as a magnetically separable visible-light photocatalyst, *Sep. Purif. Sci.* 130 (2014) 84–90.
- [16] F.P. Jiao, H.L. Song, W.J. Yang, X.Y. Jiang, X.Q. Chen, J.G. Yu, Enantioselective separation of tryptophan by Mg-Al layered double hydroxides intercalated with tartaric acid derivative, *Appl. Clay Sci.* 75 (2013) 92–99.
- [17] Y. Lu, B. Jiang, L. Fang, F.L. Ling, J.M. Gao, F. Wu, X.H. Zhang, High performance NiFe layered double hydroxide for methyl orange dye and Cr (VI) adsorption, *Chemosphere* 152 (2016) 415–422.
- [18] K. Wang, J.F. Ma, Z.S. Yao, W.Y. Zhang, S. Komarneni, Synthesis and photocatalytic properties of new ternary Ni-Fe-Cr hydrotalcite-like compounds, *Ceram. Int.* 42 (2016) 15981–15988.
- [19] X.J. Bai, C.P. Sun, D. Liu, X.H. Luo, D. Li, J. Wang, N.X. Wang, X.J. Chang, R.L. Zong, Y.F. Zhu, Photocatalytic degradation of dextrinvalenol using graphene/ZnO hybrids in aqueous suspension, *Appl. Catal. B-Environ.* 204 (2017) 11–20.
- [20] T.S. Anirudhan, F. Shainy, J. Christa, Synthesis and characterization of polyacrylic acid-grafted-carboxylic graphene/titanium nanotube composite for the effective removal of enrofloxacin from aqueous solutions: adsorption and photocatalytic degradation studies, *J. Hazard. Mater.* 324 (2017) 117–130.
- [21] G.Y. Zhang, Y.B. Sun, C.X. Zhang, Z.Q. Yu, Decomposition of acetaminophen in water by a gas phase dielectric barrier discharge plasma combined with TiO₂-rGO nanocomposite: mechanism and degradation pathway, *J. Hazard. Mater.* 323 (2017) 719–729.
- [22] W.Z. Xu, B.L. Zhang, X.L. Wang, G.S. Wang, The flame retardancy and smoke suppression effect of a hybrid containing dihydrogen phosphate anion

- modified reduced graphene oxide/layered double hydroxide on epoxy resin, *RSC Adv.* 7 (2017) 19662–19673.
- [23] M.S.S. Dorraji, A.R. Amani-Ghadim, M.H. Rasoulifard, S. Taherkhani, H. Daneshvar, The role of carbon nanotube in zinc stannate photocatalytic performance improvement: experimental and kinetic evidences, *Appl. Catal. B-Environ.* 205 (2017) 559–568.
- [24] X. Wu, D. Zhang, F.P. Jiao, S. Wang, Visible-light-driven photodegradation of methyl orange using $\text{Cu}_2\text{O}/\text{ZnAl}$ calcined layered double hydroxides as photocatalysts, *Colloid Surf. A-Physicochem. Eng. Asp.* 508 (2016) 110–116.
- [25] C.S. Zhu, J.T. Zheng, L.Y. Fang, P. Hu, Y.K. Liu, X.Q. Cao, M.B. Wu, Advanced visible-light driven photocatalyst with enhanced charge separation fabricated by facile deposition of Ag_3PO_4 nanoparticles on graphene-like *h*-BN nanosheets, *J. Mol. Catal. A-Chem.* 424 (2016) 135–144.
- [26] M.M. Gui, S.P. Chai, B.Q. Xu, A.R. Mohamed, Visible-light-driven $\text{MWCNT}/\text{TiO}_2$ core-shell nanocomposites and the roles of MWCNTs on the surface chemistry, optical properties and reactivity in CO_2 photoreduction, *RSC Adv.* 4 (2014) 24007–24013.